A Comparison of Induction-Detection NMR and Force-Detection NMR on Micro-NMR Device Design

Wen-Chieh Lin and Gary K. Fedder

March 2001
CMU-RI-TR-01-06

The Robotics Institute
School of Computer Science
Carnegie Mellon University
Pittsburgh, PA 15213

Abstract

Nuclear Magnetic Resonance (NMR) is widely used in medical diagnostics and chemical analysis. Due to rapid growing of the NMR applications, the conventional NMR systems may not fulfill the need of all applications. The development of a micro-NMR device would not only benefit the original NMR applications but could also open a door for new NMR applications. Two approaches for building a NMR system, Induction-Detection Nuclear Magnetic Resonance (IDNMR) and Force-Detection Nuclear Magnetic Resonance (FDNMR) are explored and compared in this paper. The comparison result shows that the FDNMR approach outperforms the IDNMR approach in signal-to-noise ratio when the sample radius is below 410 μm for protons and 1900 μm for chlorides. This suggests that the FDNMR approach is more appropriate for making the micro-NMR device.

I. Introduction

Nuclear magnetic resonance is a physical phenomenon that occurs when the nuclei of certain atoms are immersed in a static magnetic field and exposed to a second excitation magnetic field. Some nuclei experience this phenomenon, and others do not, dependent upon whether they possess a property called spin. The macroscopic effect of spins of nuclei can be considered as a magnetization induced by the sample, which can be manipulated by the excitation magnetic field under certain conditions. Depending on different excitation schemes, two major approaches are used to sense the motion of the magnetization. In induction-detected nuclear magnetic resonance (IDNMR), the excitation magnetic field oscillates with a specific frequency, the Larmor frequency, and a coil is used to sense the motion of the magnetization. In force-detection nuclear magnetic resonance (FDNMR), the excitation magnetic field oscillates with frequency modulated around the Larmor frequency, and a specially designed mechanical structure whose motion is coupled with the oscillation of the magnetization is used to sense the motion of the magnetization. The IDNMR approach is adopted in almost all NMR systems conventionally. On the other hand, the FDNMR approach, although first suggested by a group in Pisa early in the 1960s, had not been used until Sidles' proposal [1] in 1991, which made the revival of FDNMR approach [2].

One of the most important applications of NMR is magnetic resonance imaging (MRI), which is widely used in medical diagnostics. Another important application of NMR is spectroscopy, which is a technique that can determine a sample‘s chemical composition. It is widely used in research laboratories to analyze the chemical or biological samples. NMR can also be used as a detection mechanism, such as oil well logging where companies used it to characterize earth strata. In addition to these applications, more and more applications of NMR will be explored as NMR development makes these systems more affordable and accessible.

As the applications of NMR expand, the demand of more appropriate and convenient equipment designed for a specific application is increasing. For example, in some applications of chemical or biological analysis, such as microspectroscopy and NMR-detected microseparation, the test samples are very small—typical volume is around or below a microliter. To exploit these volume-limited samples efficiently, the usual NMR device, which is designed for large samples, is not appropriate. An important feature of NMR is that its signal-to-noise ratio (SNR) is linearly dependent on the volume of the sample. Therefore, a micro-NMR device designed for micro-samples is necessary. Conventional NMR equipment, including desktop NMR equipment, are relatively large and their applications are limited because of the size. The development of a highly integrated micro-NMR device could further expand the application realm of NMR [3].

Toward the goal of making a micro-NMR device that integrates the full function of the NMR system, some researchers have started the development from the NMR probe (microcoil) design, which is critical for a micro-NMR device since the SNR of the device is mostly determined by the probe design. Peck et al. [4] first used a micromachining technique to fabricate a 100 μm inner diameter planar spiral microcoil on a gallium

arsenide substrate. The microcoil was used in ^{1}H NMR spectroscopy experiments with a 7.05 T static magnetic field. To reduce the resistance of the coil, which improves the SNR of the system, the microcoil was made of gold. A single-shot SNR of 2.5 was achieved in the experiments. A further improvement of single-shot SNR to 25 using a 60 μm inner diameter microcoil, which was optimized in geometry design for maximizing SNR, had been reported later [5].

Recently, Boero et al. [6][0] integrated the microcoil with CMOS integrated circuits for NMR signal detection and amplification. They used the device as an NMR magnetometer, which is commonly used for high-precision measurements of static magnetic field. In this special application of NMR, a fixed and sensitive sample is used and the static magnetic field strength is obtained by measuring the resonance frequency of magnetization of the sample. Although a full integration of an NMR system, including probe, amplifier and signal processing circuits, has not been achieved, the partial integration done by Boreo et al. shows a promising way to reach the final goal.

Similar to the development of conventional NMR system, all developments of a micro-NMR device so far are following the mainstream IDNMR approach. Although there is a much richer study of development of a micro-NMR device based on the IDNMR approach, we would like to know if FDNMR is a better approach to build a micro-NMR device. In this paper, we will provide an initial evaluation of these two approaches. We first briefly review the working principles of IDNMR and FDNMR in section II and III. Their design considerations for making an NMR device are also discussed. In section IV, we compare the SNR performance of IDNMR and FDNMR due to scaling. Finally, we conclude in section V with a comparison and discuss the future work of development of the micro-NMR device.

II. Induction-Detection Nuclear Magnetic Resonance

1. Principles of IDNMR

NMR is a quantum phenomenon. When atoms possessing spin property are placed in a static magnetic field $\mathbf{B_0}$, the nucleus of each atom has a magnetic moment whose orientation is quantized. The number of quantized states is defined by a half-integer I_s, called spin number. For ^{1}H nucleus (proton), the spin number is $\frac{1}{2}$ and thus the orientation can be either parallel ($-\frac{1}{2}$) or antiparallel ($\frac{1}{2}$) to the static field with parallel case having slightly lower energy. In the thermal equilibrium state, the number of protons in lower energy state is only slightly larger than that in higher energy state since the energy difference is very small compared to the average thermal energy of the system. The energy difference can be calculated by $\Delta E = h\nu_0$, where h is the Planck constant, and ν_0 is the transition frequency. One of the unique features of the magnetic resonance is that the transition frequency $\nu_0 = \gamma \cdot B_0 / 2\pi$, called the resonance frequency or Larmor frequency, is proportional to the applied field and the gyromagnetic ratio, which is a

property of the atoms—in this case, γ is the gyromagnetic ratio of the protons. It is this property that makes the NMR capable of detecting or analyzing the chemical composition of a sample. Protons may be excited into the higher energy state if an electromagnetic wave is applied to the system, provided that its frequency v obeys the Bohr relationship $\Delta E = hv$ and that a proper arrangement is used. A usual way to do this is applying an excitation magnetic field whose direction is perpendicular to the static magnetic field and its magnitude oscillates at the Larmor frequency v_0.

The macroscopic effect of nuclear spins, when only a static magnetic field exists, can be considered as a magnetization whose direction is collinear with the static magnetic field and its value can be obtained from a general expression of the Curie law,

$$M_0 = N_{atoms/volume} \frac{\gamma^2 \hbar^2 B_0 I_s (I_s + 1)}{3 k_B T}$$

where $N_{atoms/volume}$ is the number of atoms per unit volume, $\hbar$ is the Planck constant divided by 2π, k_B is the Boltzmann constant ($k_B = 1.3806 \times 10^{-23} JK^{-1}$), and T is the absolute temperature in kelvin. If an oscillation field is added, the magnetization is subjected to a precessional motion around $\mathbf{B_0}$. This motion can be explained on the basis of the angular momentum theorem and occurs at a frequency equal to the Larmor frequency. The angle between the magnetization and $\mathbf{B_0}$ is determined by the amplitude and duration of the oscillation field $\mathbf{B_1}$.

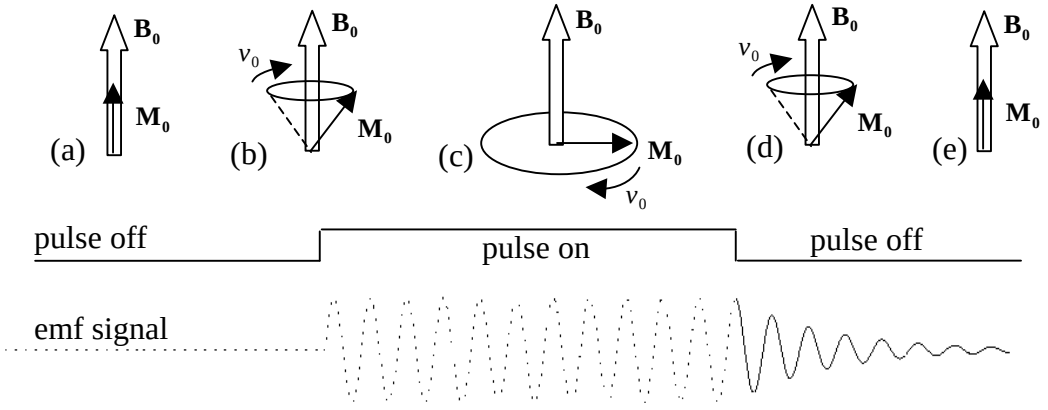

Fig. 1. The evolution of magnetization and emf signal during an excitation pulse. (a) the equilibrium state: when only $\mathbf{B_0}$ exists (pulse off), $\mathbf{M_0}$ is collinear with $\mathbf{B_0}$. (b) when the pulse is just on, $\mathbf{B_1}$ perturbs $\mathbf{M_0}$ and causes it precess around $\mathbf{B_0}$ with frequency v_o. (c) After a very short period, $\mathbf{M_0}$ is displaced onto the coil plane. (d) Once the pulse is off, $\mathbf{M_0}$ starts to back to the equilibrium state and the induced emf signal is exponentially decayed. (e) After a relaxation period, $\mathbf{M_0}$ recovers to the equilibrium state. The emf signal in the dashed line represents that the coil is served as an excitation coil when the pulse is on and no signal is detected until the pulse is off.

An IDNMR system requires a static magnetic field, an rf coil, and electronics to run the experiment and analyze the data. The static magnetic field is often contributed by a permanent magnet that provides strong field intensity at the range of several Teslas. The rf coil generates the oscillation magnetic field, $\mathbf{B_1}$, that is transverse on the plane perpendicular to $\mathbf{B_0}$, which we call the coil plane. In the pulse NMR approach, which is commonly used in IDNMR systems, the excitation field is turned on and off by a pulse signal. When the pulse is on, the rf coil generates the oscillation field which displaces the magnetization onto the coil plane; when the pulse is off, the rf coil detects the electromotive force (emf) induced by the precession of magnetization[1]. Fig. 1 shows the magnetization at different states of excitation and the emf signal sensed by the rf coil. The emf signal is at maximum when the magnetization is displaced on the coil plane and its amplitude starts to decay once the pulse is off because the magnetization starts to back to the equilibrium state at that moment. The pulse width that exactly causes $\mathbf{M_0}$ to precess in the coil plane, is called a $\pi/2$ pulse, since $\mathbf{M_0}$ makes a $\pi/2$ angle with $\mathbf{B_0}$. Therefore, the emf signal sensed by the coil is an exponentially damped sinusoidal signal whose frequency is close to the Larmor frequency. The detected emf signal is called the free induction decay (FID). It is actually a synthesis of signals contributed by each part of the sample. For a uniform static magnetic field, the signal coming from each part has the same frequency, and the synthesized FID signal has a single frequency constitution, i.e., the Larmor frequency. Thus, atoms of specific elements can be detected by analyzing the frequency spectrum of the FID. If a linear-gradient magnetic field is used, the position information can be encoded in the field gradient. The frequency spectrum of the FID would reflect the positional information of the atoms. Depending on whether a 1-D gradient or 2-D gradient field is used, an NMR spectroscopy or "magnetic resonance imaging" (MRI) can be obtained.

2. The SNR of IDNMR and the modeling of microcoil

The SNR is an accepted standard for measurement quality of an NMR system. Hoult and Richards [8] developed a concise closed-form expression for the IDNMR SNR.

$$SNR_i = \frac{EMF\ signal}{Noise} = \frac{\omega_0 \frac{B_1}{I} M_0 V_s}{\sqrt{4k_B T r_{coil} \Delta f}} \tag{1}$$

The numerator of Eq. (1) represents the emf voltage induced in the coil following the application to the sample of a $\pi/2$ excitation pulse. The emf voltage is determined by the sample characteristics and coil characteristics. The former includes the Larmor frequency in radians ω_0, the magnetization magnitude M_0, and the sample volume V_s; the latter includes the magnitude of the transverse magnetic field $\mathbf{B_1}$ induced in the rf coil by a unit dc current I. This equation assumes the same coil is used for both excitation and detection. The denominator of Eq. (1) is the thermal noise measured over a defined

[1] For some NMR experiments, two or more rf coils may be used: some for excitation and others for pickup.

spectral bandwidth (Δf) at sample temperature (T). The thermal noise is induced by the coil resistance r_{coil}.

The coil design is a critical part to achieve a high SNR in building an NMR device. Specifically, the SNR of a microcoil in the NMR device is determined by the electrical property of the coil. A good model of the microcoil is important. The electrical model of a 3-layer planar microcoil will be described here. Also, the geometry design considerations of the microcoil will be briefly discussed.

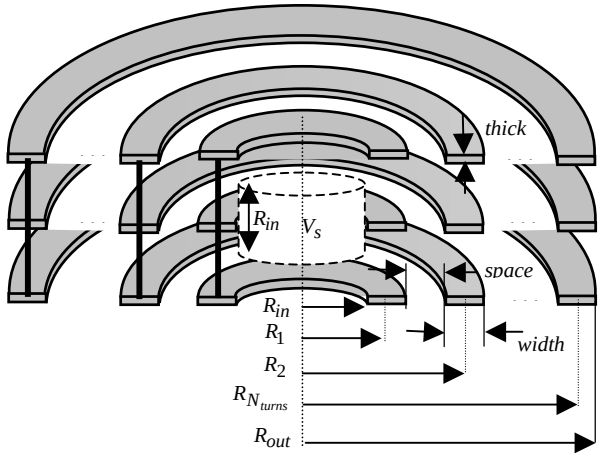

Fig. 2. A circular planar microcoil consists of three layers connected in parallel.

Fig. 2 shows a microcoil consisting of three layers that are connected by wires. On each layer, there are N_{turns} turns. R_n, R_{in}, and R_{out} are the center radius of the coil at the nth turn, the inner coil radius, and the outer coil radius, respectively. Here we define the coil sensitivity as the magnitude of the magnetic field generated by a unit dc current I in the coil. The coil sensitivity calculated on the axis of the coil center with distance Z from the coil center is [20]

$$\frac{B_1}{I} = \sum_{n=1}^{N_{turns}} \frac{\mu_0 {R_n}^2}{2({R_n}^2 + Z^2)^{3/2}} \qquad \xrightarrow{Z=\frac{1}{2}R_{in}} \qquad \frac{B_1}{I} = 0.8\sqrt{5}\mu_o \sum_{n=1}^{N_{turns}} \frac{1}{R_n} \tag{2}$$

From Eq. (2), we can approximate the effective sample volume by bounding it within the cylindrical region whose bottom and top are above and below the coil surface by half of the inner coil radius, respectively. This is because the coil sensitivity drops approximately 30 percent at the positions $Z = \pm R_{in}/2$. Thus, the sample volume is defined as $V_s = \pi \cdot {R_{in}}^3$. For conservative design, the sensitivity of the whole coil is represented by its minimum value at $Z = \pm R_{in}/2$. The inductance of the microcoil is approximated by

$$L_{coil} = \frac{B_1 \cdot Area_{coil}}{I} = 0.8\sqrt{5}\mu_0 \pi \sum_{n=1}^{N_{turns}} R_n \tag{3}$$

Detailed calculation of the resistance of the coil should take into account the conductive losses of the coil as well as magnetic (eddy current) and dielectric losses in the sample and surrounding structures. For microcoil design, since the sample volume is very small (microliter or less), the dielectric losses in the sample can be ignored and the conductive losses becomes the major source of the noise [9]. When calculating the conductive losses, both the dc resistance and ac resistance, including the skin effect and proximity effect, should be considered; however, if the wire width/height of the coil is less than twice the skin depth, these two effects are negligible [10]. For aluminum, which is commonly used as the material of metal layers in CMOS process, the skin depth is 12 μm at 50 MHz, and 37 μm at 5 MHz. Hence, under the skin depth, the value of coil resistance approaches its dc resistance,

$$r_{coil} = \frac{Length}{\sigma \cdot A_{wire}} = \frac{\sum_{n=1}^{N_{turns}} 2\pi \cdot R_n}{\sigma \cdot width \cdot thick \cdot N_{layers}} \tag{4}$$

where σ is the conductivity of the wire, A_{wire} is the cross-sectional area of the coil wire and N_{layers} is the number of metal layers of the microcoil. The amplitude of the emf signal is then given by [0]

$$EMF = \omega_0 \frac{B_1}{I} M_0 V_s \tag{5}$$

Using Eq. (3) and Eq. (4), the quality factor can be obtained by $Q = \omega_0 \cdot L_{coil} / r_{coil}$. In macro-scale coils, this emf voltage is further amplified by the quality factor when the voltage is measured at the terminals of the coil; however, this is usually not the case in the microcoil since its quality factor is often smaller than one. Hence, the main considerations of microcoil design are how to reduce the coil resistance and increase the coil sensitivity. Regarding the first consideration, the coil wire (track) should have the cross-sectional area as large as possible, and the total wire length as short as possible. For this reason, we adopt the three-layer coil to increase the cross-sectional area. For the second consideration, an intuitive thinking is the outer turns of the coil contribute less for the coil sensitivity, but would increase the coil resistance; however, decreasing the number of coil turns reduces sensitivity. A better way to resolve the problem is to increase the height of the coil wire, which can reduce the coil resistance and maintain the coil sensitivity.

3. The SNR of IDNMR due to scaling

A scaling law of SNR regarding the change of the coil size will be derived here. Since the scaling is the main interest, we can exclude other factors unrelated to scaling in Eq. (1) and express it as follows:

$$SNR_i \propto \frac{B_1}{I\sqrt{r_{coil}}} V_s \tag{6}$$

To further simplify Eq. (6), the geometry of the coils must be specified. The planar circular microcoil as shown in Fig. 2 will be considered here[2]. Using Eq. (2), the coil sensitivity due to scaling is expressed as follows:

$$\frac{B_1}{I} = 4 \cdot 5^{-\frac{3}{2}} \mu_o \sum_{n=1}^{N_{turns}} \frac{1}{R_n} \propto \frac{N_{turns}}{L} \tag{7}$$

where we assume that the radius of each turn does not vary significantly and is approximated as an average coil radius R. L represents the length scale of a coil. Similarly, the coil resistance due to scaling is obtained by

$$r_{coil} = \frac{N_{turns} 2\pi \cdot R}{\sigma \cdot A_{wire} N_{layers}} \propto \frac{N_{turns} L}{A_{wire}} \tag{8}$$

Combining Eqs. (6)~(8), the SNR equation regarding the scaling is expressed as

$$SNR_i \propto V_s \sqrt{\frac{N_{turns} A_{wire}}{L^3}} \tag{9}$$

The number of turns of coil is related to the cross-sectional area of the coil wire (A_{wire}). If A_{wire} is scaled with the coil size, then N_{turns} is fixed; however, if for some reason, e.g., a fabrication constraint in manufacture process, A_{wire} can't be increased arbitrarily, then it should be considered as a constant when scaling. In this case, N_{turns} would increase proportionally to the coil size. Another consideration is the sample volume. Usually, we can obtain as much sample as we want. Under this condition, the sample volume can be scaled with the coil size. In some cases, however, the sample volume is limited, e.g., the microspectroscopy of some biological samples or real time analysis of fluid samples. Taking into account these conditions, the scaling law of SNR based on Eq. (9) is shown in Table 1.

$SNR_i \propto L^{\beta}$		Sample Volume	
		Scaled	Fixed
Cross-sectional Area of Wire	Scaled	$\beta = \frac{5}{2}$	$\beta = -\frac{1}{2}$
	Fixed	$\beta = 2$	$\beta = -1$

Table 1: Scaling law of SNR under different conditions

[2] Although the scaling for a solenoidal coil is not shown here, the same scaling law can be obtained by similar derivation.

It is interesting to note that shrinking the coil size doesn't always win. The best coil is always one that exactly fits the sample.

Another interesting question here would be: does the SNR benefit from the replacement of a single coil with a coil array? From the previous derivation, we know that

$$SNR_i = K \cdot L^{\beta} \tag{10}$$

where K is a constant and β is as defined in Table 1. If we replace a coil with N small coils to form a coil array, which occupies the same area as that by the original one, the SNR of each individual coil is

$$\frac{SNR_s}{SNR_o} = \frac{K(\frac{L}{\sqrt{N}})^{\beta}}{KL^{\beta}} = (\frac{1}{\sqrt{N}})^{\beta} \tag{11}$$

where SNR_s and SNR_o are the SNR of the small coil and original coil, respectively. Assuming the interaction between the magnetic fields of these small coils is negligible and the noise in every small coil is uncorrelated with one another, the total SNR of the coil array is

$$SNR_{total} = \sqrt{N} \cdot SNR_s = \sqrt{N}^{1-\beta} SNR_o \tag{12}$$

The effect of using a coil array regarding the scaling of the coil size can be summarized in Table 2. The result shows that if the sample volume is limited, the total SNR of the coil array increases as the number of coils increases; however, if the sample volume can be scaled with the size of the coil, using a coil array would decrease the SNR instead. The results in Table 1 and Table 2 actually reflect an important fact of the NMR system: its SNR is highly dependent on the sample size.

$\frac{SNR_{total}}{SNR_o} \propto N^{\alpha}$		Sample Volume	
		Scaled	Fixed
Cross-sectional Area of Wire	Scaled	$\alpha = -\frac{3}{4}$	$\alpha = \frac{3}{4}$
	Fixed	$\alpha = -\frac{1}{2}$	$\alpha = 1$

Table 2: Scaling of the SNR when a coil array is used

III. Force-detection Nuclear Magnetic Resonance

Conventionally, the NMR has been developed almost entirely with magnetic induction as the means of detection; however, magnetic induction is not the only way to detect magnetic resonance. Sidles [1] first proposed to couple the harmonic motion of the nuclear spin to the motion of a mechanical oscillator. Based on Sidles' proposal, the first

experiment, which is now called magnetic resonance force microscopy (MRFM), was achieved by Rugar et al. [11]. In the experiment, the electron spin resonance (ESR) was detected. They used cyclic adiabatic fast passage to modulate the equilibrium longitudinal magnetization at the audio frequency resonance of a sample-on-cantilever assembly. A large static magnetic field gradient, induced by the nearby ferromagnetic particle, was used to provide the magnetic force and to vary the resonance condition across the sample. Since then, the method has been extended to ^{1}H NMR [12] using ultra-thin cantilevers and to ^{1}F NMR [13] at low temperature. Recently, Leskowitz et al. [14] proposed a force-detection NMR method without field gradient. In contrast to other FDNMR methods, their method is characterized by better observation of magnetization, enhanced resolution, and no gradient (BOOMERANG). In the following, we will briefly review the principles of FDNMR and BOOMERANG, and discuss about the design considerations in BOOMERANG.

1. Principles of FDNMR

The force detected in FDNMR [15] is given by

$$\mathbf{F} = \nabla(\mathbf{m} \cdot \mathbf{B}) \tag{13}$$

where $\mathbf{m}$ is a magnetic moment due to nuclear spins, and $\mathbf{B}$ is an inhomogeneous magnetic field. The spin magnetic moment is $\mathbf{m} = \mathbf{M}_0 V_s$, where $\mathbf{M}_0$ is the nuclear magnetization of the sample and V_s is the sample volume. From Eq. (13), we know that a field gradient is needed to generate the force. Also, an excitation scheme of magnetization is needed to retain the resonance that is coupled to the resonance of the mechanical oscillator. Based on these considerations, a basic configuration of FDNMR consisting of a cantilever, an rf coil, and a ferromagnetic particle is shown in Fig. 3. In addition, a magnetic field along the z direction, which is not shown in the figure, is used to polarize the nuclei in the sample. The rf coil mounted close to the sample provides an oscillating field to excite magnetic resonance. In the absence of rf excitation, a strong field gradient generated by the nearby ferromagnetic particle causes a measurable deflection of the cantilever. The deflection can then be sensed by a fiber-optic interferometer. When the rf coil turns on, a special modulation technique is applied to cause the magnetization to oscillate along the $\mathbf{z}$ direction. The resonant frequency of the cantilever is designed as the same frequency of the oscillation of the magnetization. By sensing the vibration frequency of the cantilever, the magnetization due to electron or nuclear spins can be detected.

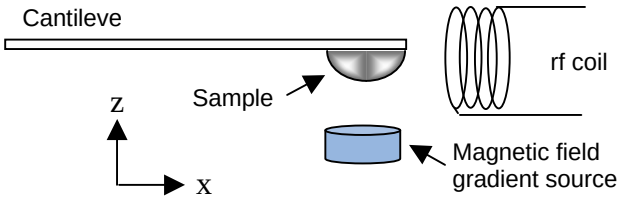

Fig. 3. A basic configuration of FDNMR

The modulation scheme is based on the adiabatic fast passage [16] method. Under the adiabatic condition, the nuclear magnetization, viewed in a reference frame rotating at the frequency of the rf excitation, can be made to follow the direction of the effective field $\mathbf{B}_{eff}$, where

$$\mathbf{B}_{eff} = B_1\hat{\mathbf{x}} + (B_0 - \omega/\gamma)\hat{\mathbf{z}} \tag{14}$$

Here, B_0 is the magnitude of the static field, B_1 is the amplitude of the applied rf magnetic field, which, in the rotation frame, is a constant field in the $\hat{\mathbf{x}}$ direction, ω is the rf frequency, and γ is the gyromagnetic ratio. Rather than set the rf frequency around the Larmor frequency ($\omega \cong \gamma \cdot B_0$) as in IDNMR, the rf frequency in FDNMR is modulated as $\omega(t) = \omega_0 + \Delta\omega(t)$ ($\omega_0 = \gamma \cdot B_0$ is the Larmor frequency; $\Delta\omega = \Omega \sin \omega_c t$, ω_c is the cantilever resonance frequency). The $\mathbf{B}_{eff}$ reduces to

$$\mathbf{B}_{eff} = B_1\hat{\mathbf{x}} - \frac{\Delta\omega(t)}{\gamma}\hat{\mathbf{z}} \tag{15}$$

If the frequency modulation is at a sufficiently slow rate so that the adiabatic condition is satisfied [16], the nuclear magnetic moment will follow the direction of $\mathbf{B}_{eff}$. Additionally, if the peak frequency deviation (Ω) is large enough, the effective magnetic field, $\mathbf{B}_{eff}$, will oscillate almost parallel to the $\hat{\mathbf{z}}$ direction. The magnetic moment, according to the adiabatic condition, would oscillate in the same manner.

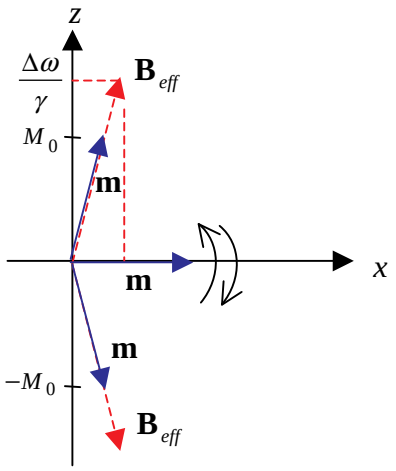

Fig. 4. The vector diagram of $\mathbf{B}_{eff}$ and $\mathbf{m}$

This creates a cyclic force on the sample and causes the cantilever to vibrate. In this case, since the field gradient is along the $\hat{z}$ direction only, the generated force given by Eq. (13) can be simplified as

$$F_z(t) = m_z(t)\frac{\partial B_z}{\partial z} \tag{16}$$

where $m_z(t)$, as shown in Fig. 4, is given by

$$m_z(t) = -M_0 \frac{\Delta\omega(t)/\gamma}{\sqrt{(\Delta\omega(t)/\gamma)^2 + B_1^{\,2}}} \tag{17}$$

2. Principles of FDNMR without Field Gradient – BOOMERANG [14]

The basic idea of BOOMERANG is to switch the roles of magnetic field and magnetic moment in conventional FDNMR[3]. That is, the gradient of the sample field (magnetic moment) is used to generate the force instead of the gradient of the magnetic field. Reflecting the exchange of roles, the magnet in BOOMERANG is mounted on a mechanical structure, such as cantilever or membrane, while the sample is not fixed and can be replaced freely for different experiments. In conventional FDNMR, due to the field gradient, only a slice of sample on which the magnetic field is uniform is used in detection; however, since the magnetic field in BOOMERANG is homogeneous across the sample, the signal from the whole sample can be utilized. This makes BOOMERANG have higher sensitivity than the conventional FDNMR. In the following, the design equations used in BOOMERANG will be briefly reviewed.

Consider a spherical sample shown in Fig. 5. The exterior field of the sample is the same as that of a point dipole at its center. In this case, the force $\mathbf{F_d}$ on a ferromagnetic sensor dipole $\boldsymbol{\mu}_\mathbf{d}$ aligned along the z-axis and located at arbitrary position $\mathbf{r}$ in the field of the sample dipole $\boldsymbol{\mu}_\mathbf{s}$ is given by [14] [17]

$$\mathbf{F_d} = \nabla(\boldsymbol{\mu}_\mathbf{d} \cdot \mu_0 \boldsymbol{\mu}_s) = \frac{\mu_0}{4\pi}\frac{|\boldsymbol{\mu}_\mathbf{s}||\boldsymbol{\mu}_\mathbf{d}|}{|\mathbf{r}|^4}\left[\cos\theta(9-15\cos^2\theta)\hat{\mathbf{z}} + \sin\theta(3-15\cos^2\theta)\hat{\boldsymbol{\rho}}\right] \tag{18}$$

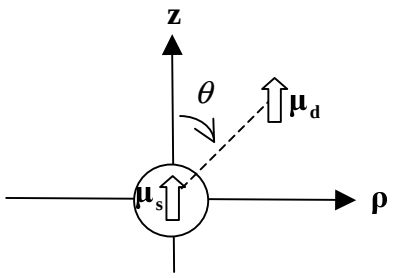

Fig. 5. A sensor dipole in the gradient field of a sample dipole

[3] If we observe from Eq. (13), $\mathbf{m}$ and $\mathbf{B}$ are interchangeable.

For a uniformly magnetized spherical sample, the total magnetic force between sample and surroundings is obtained by replacing $\boldsymbol{\mu}_\mathbf{d}$ in Eq. (18) with the dipole element $d\boldsymbol{\mu}_\mathbf{d}$, and integrating over the surroundings. Since we are interested in generating the force that oscillates along the z-axis, we will only consider the z-component of $\mathbf{F}_\mathbf{d}$ hereafter. From Eq. (18), we know that the z-component of $\mathbf{F}_\mathbf{d}$ is a function of θ, and has its direction of force toward the sample for a cone region defined by $|\theta| \le 39.2°$. We can design the magnet shape to fully utilize this region to maximize the magnetic force. When this is the case, a conical magnet would be the best choice; however, for the simplicity of fabrication, a cylindrical magnet detector is adopted in BOOMERANG. Since the spherical sample of volume V_s has uniform magnetization $\mathbf{M}_\mathbf{0}$, $|\boldsymbol{\mu}_\mathbf{s}|$ in Eq. (18) can be replaced by $M_0 V_s$, and the magnetic force (z-component) between the sample and the detector magnet can be calculated as

$$\begin{aligned} F &= \int_{V_d} \frac{\mu_0}{4\pi} \frac{M_0 V_s M_d}{r^4} \cos\theta (9 - 15\cos^2\theta) dV_d \\ &= \frac{\kappa_F \mu_0 M_0 V_s M_d}{R_{\max}} \end{aligned} \tag{19}$$

wher V_d is the volume of the detector magnet with magnetization M_d, $R_{\max}$ is the distance from the center of the sample to the near face of the detector magnet, and κ_F is a dimensionless constant that characterizes the geometry of the particular design.

3. Design considerations in BOOMERANG

The main design issues in BOOMERANG are the magnet design and mechanical structure design. The magnet design actually consists of the detector magnet and the magnet that is used to polarize the nuclei in the sample. For the latter one, the design objective is to building a homogeneous field across the sample such that the whole sample can be fully used. For the detector magnet design, its shape is important. The radius of the cylindrical magnet is limited by $R_{\max}$ because of the limited cone region ($|\theta| \le 39.2°$). Here, $R_{\max}$ is dominated by the radius of the spherical sample (R_s) and must include the headroom for the oscillation of the mechanical structure. The height of the magnet is the only unconstrained factor for optimization of the SNR of the system. Although the optimum height may not seem clear here, an intuitive thinking[4] about the height is: if the height is too large, the additional mass of the mechanical oscillator contributes less to the magnetic force but reduces the quality factor, which decreases the SNR of the system. On the other hand, if the height is too small, the weak magnetic force will cause a poor SNR. Thus, there exists an optimum value of height that maximizes the SNR of the system.

[4] This is similar to coil sensitivity and coil resistance dilemma in the microcoil design. The height of the magnet is analogous to the outer radius of the coil.

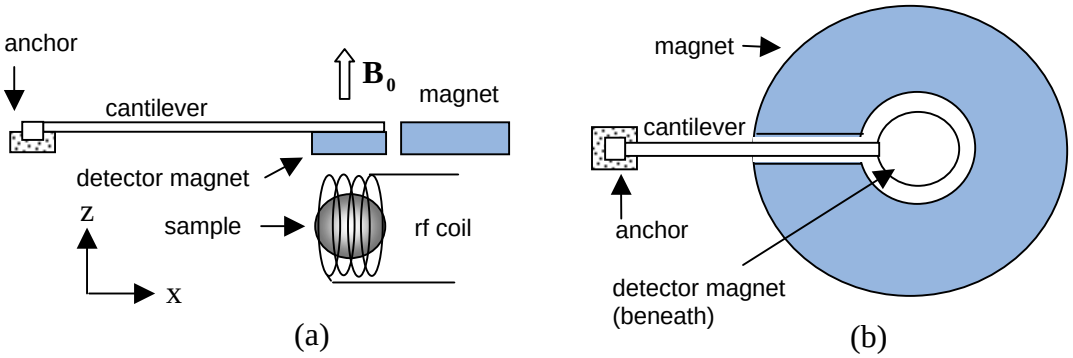

Fig. 6. A cantilever implementation of BOOMERANG: (a) side-view, (b) top-view

To further clarify the design issues, a BOOMERANG implementation based on the cantilever structure is discussed here. Fig. 6 shows the configuration of the implementation. The material of the detector magnet and the surrounding magnet are the same and the gap between them is small as shown in Fig. 6(b). The reason for setting a small gap is to make the generated field across the sample as uniform as possible. Assume the quality factor Q and the resonance frequency f of the cantilever are given. The length of the cantilever, which is modeled as a uniform beam with concentrated load at the free end is determined by [18]

$$l = \left(\frac{1.732}{2\pi \cdot f}\right)^{\frac{2}{3}} \left(\frac{EI}{m_d + 0.236 m_c}\right)^{\frac{1}{3}} \tag{20}$$

where E is the modulus of elasticity, $I = w_b \cdot {t_b}^3 / 12$ is the area moment of inertia of the beam with width w_b and thickness t_b, m_d and m_c are the mass of detector magnet and cantilever, respectively. The spring constant k is approximated by dividing the end-load by the maximum deflection at the end of the cantilever:

$$k = \frac{3EI}{l^3} \tag{21}$$

The effective mass of the cantilever is calculated as

$$m_{eff} = \frac{k}{(2\pi \cdot f_1)^2} = m_d + 0.236 m_c \tag{22}$$

and the damping constant of the cantilever is given by

$$B_{damp} = m_{eff} \frac{2\pi \cdot f}{Q} \tag{23}$$

The major noise source in BOOMERANG is the Brownian motion of the mechanical oscillator, which is similar to the thermal noise in IDNMR. The Brownian noise is:

$$F_f = \sqrt{4k_B T B_{damp} \Delta f} \tag{24}$$

where k_B is the Boltzmann constant, T is the absolute temperature, and Δf is the detection bandwidth of the system. Combining Eqs. (19) through (24), the SNR of BOOMERANG based on a cantilever oscillator can be expressed as

$$SNR_f = \frac{Q}{f} \frac{\kappa_f \mu_0 V_s M_o M_d}{\sqrt{8k_B T \pi (m_d + 0.236 m_c) R_{\max}}} \tag{25}$$

where the detection bandwidth is assumed to be limited by the quality factor $Q = f/\Delta f$. The maximum deflection due to force F is obtained by

$$Z_{\max} = Q \frac{F}{k} \tag{26}$$

IV. Comparison of the SNR of IDNMR and FDNMR due to Scaling

After studying the scaling properties of SNR of IDNMR and FDNMR, one might ask: which approach should be adopted in building a micro NMR device? A comparison result of these two approaches is provided based on the scaling properties and design considerations described in last two sections. All geometry parameters are scaled except the cross-sectional area of coil wire and the thickness of cantilever, which are fixed since they can't be scaled arbitrarily in a microfabrication process. The aspect ratios of scaled parameters to the controlled variable are listed in Table 3. The aspect ratio used in IDNMR is chosen from our simulation results for microcoil design, while those used in FDNMR is a numerical example used in BOOMERANG. An additional assumption for FDNMR is that the quality factor and resonance frequency of the cantilever are also fixed. The detection bandwidth of IDNMR is assumed as 1000 Hz.

	IDNMR	FDNMR
Non-scaled parameters	$thick = 0.5$ μm $width = 5$ μm $\Delta f = 1000$ Hz	$t_b = 5$ μm $Q = 100$ $f = 500$ Hz
Values of the scaled parameters when controlled variable R_s =1 μm (aspect ratio to R_s)	$R_{out} = 1.25$ μm	$w_b = 2/15$ μm $R_d = 2/3$ μm $h_d = 3/5$ μm $R_{\max} = 17/15$ μm
Controlled variables	$R_{in} = R_s$	R_s

Table 3: Assumptions for non-scaled and scaled parameters used in comparison

For the material property, the material of coil used in IDNMR is aluminum (conductivity $\sigma = 3.55\times10^{7}\ \Omega^{-1}\cdot\mathrm{m}^{-1}$); in FDNMR, the material of the detector magnet and cantilever are cobalt platinum (density $\rho_d = 11\,\mathrm{g/cm}^3$, residual induction 0.45 T [19]) and silicon dioxide (density $\rho = 2.5\,\mathrm{g/cm}^3$, the modulus of elasticity $E = 60\,\mathrm{GPa}$), respectively. Two samples are used in the comparisons: one is the proton sample, and the other is the chloride sample (1% KCl by mass in H_2O). The static magnetic field that polarizes the nuclei of the samples is 1 T, and the sample temperature is 290 K.

Sample radius (m)	SNR	emf (V)	SNR	Force (N)	Deflection (m)	Magnet Radius (m)	Cantilever length (m)
1.00E-04	1.48E+00	1.67E-08	1.31E+01	1.99E-12	2.19E-09	6.67E-05	6.50E-04
4.10E-04	2.65E+01	1.31E-06	2.65E+01	3.35E-11	5.35E-10	2.73E-04	2.54E-04
1.00E-03	1.55E+02	1.84E-05	4.14E+01	1.99E-10	2.19E-10	6.67E-04	1.40E-04
1.00E-02	1.56E+04	1.85E-02	1.31E+02	1.99E-08	2.19E-11	6.67E-03	3.02E-05

Table 4: Comparison of IDNMR and FDNMR on the proton sample

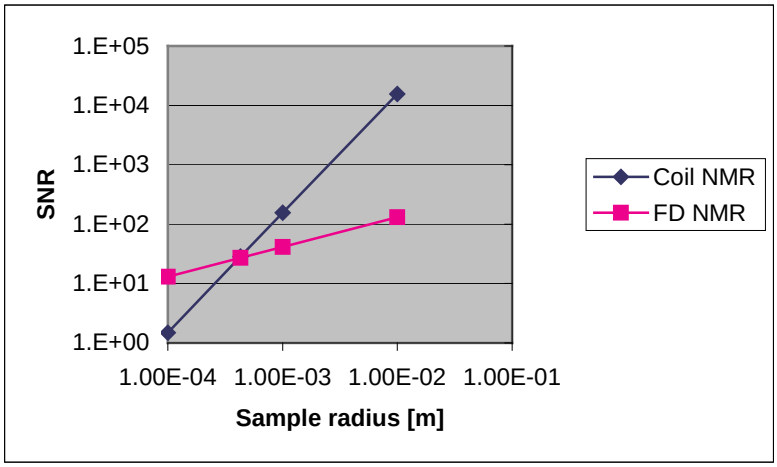

Fig. 7. SNR plot of IDNMR and FDNMR for the proton sample

Sample radius (m)	SNR	emf (V)	SNR	Force (N)	Deflection (m)	Magnet Radius (m)	Cantilever length (m)
1.00E-04	1.68E-05	1.90E-13	1.52E-03	2.31E-16	2.53E-13	6.67E-05	6.50E-04
1.00E-03	1.76E-03	2.09E-10	4.80E-03	2.31E-14	2.54E-14	6.67E-04	1.40E-04
1.90E-03	6.38E-03	1.44E-09	6.62E-03	8.34E-14	1.34E-14	1.27E-03	9.13E-05
1.00E-02	1.77E-01	2.11E-07	1.52E-02	2.31E-12	2.54E-15	6.67E-03	3.02E-05

Table 5: Comparison of IDNMR and FDNMR on the chloride sample

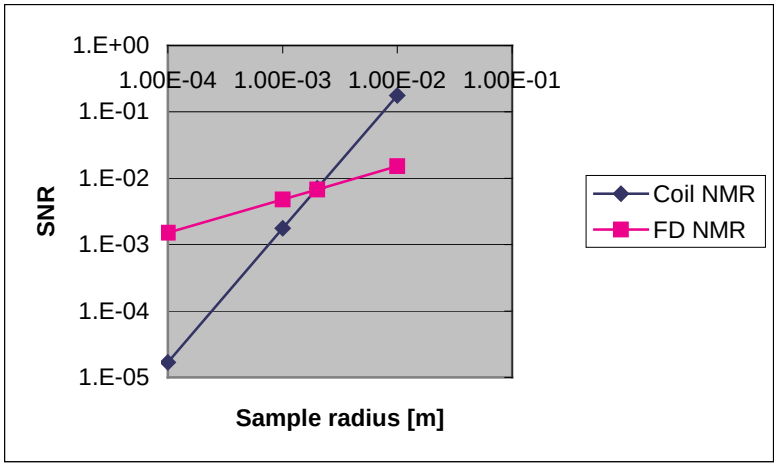

Fig. 8. SNR plot of IDNMR and FDNMR for the chloride sample

Table 4 and Fig. 7 shows the comparison result on the proton sample. In Fig. 7, we find that the FDNMR approach has higher SNR when sample radius is less than 410 μm. For chlorides, a similar result is also obtained, which shows the SNR of FDNMR is better than IDNMR as long as the sample radius is less than 1900 μm. A model validation problem should be noted here. Since we model the cantilever as a beam with a concentrated load at its free end, the radius of the detector magnet mounted on the cantilever should be much less than the cantilever length. Because we limit the frequency and quality factor of the cantilever in assumptions, the cantilever length calculated in Eq. (20) is not always practical[5]. Therefore, when viewing the result in Table 4 and Fig. 7, the data for which the sample radius is greater than 410 μm can only be considered as a trend of the curve, not the real data. Even though, the result in Table 4 is still useful because the valid region covers the main design range of a microcoil. Similarly, we can consider the comparison data for the chloride sample only valid when the sample radius is less than 410 μm.

A great advantage of FDNMR over IDNMR is its higher SNR for NMR experiments with small sample size and low Larmor frequency ω_0, which corresponds to low static magnetic field B_0 or low gyromagnetic ratio γ. This feature can be observed from their SNR expressions. In Eq. (1), the SNR is proportional to $\omega_0^{\,2}$ ($M_0 \propto \omega_0$), and in Eq. (25), it is proportional to ω_0. If we observe Fig. 7 and Fig. 8 at small radius, the ratio of the SNR of FDNMR to that of IDNMR for chloride is almost 10 times the SNR ratio for protons. The ratio of FDNMR SNR to IDNMR SNR is proportional to the gyromagnetic ratio of protons to chlorides ($\gamma_H = 2.675\times10^8$ rad/s·T, $\gamma_{Cl} = 2.621\times10^7$ rad/s·T).

Another advantage of FDNMR is its frequency modulation scheme. Using this modulation scheme, the resonance frequency of the mechanical structure can be designed

[5] This problem can be improved by increasing the thickness of the cantilever such that the geometry of the cantilever is more realistic when the dimension is enlarged with the sample radius.

with a very high quality factor, which is not possible for the micro NMR device implemented by the inductively detected approach.

V. Conclusion

The development of a micro-NMR device could reduce the cost and enhance the flexibility of the NMR system. This not only improves the SNR of the NMR systems for micro-samples but also provide the opportunities to explore new applications of the NMR. While most research on micro-NMR adopts the traditional approach—IDNMR to develop their system—the initial evaluation in this paper shows that FDNMR provides better SNR performance for building the micro-NMR device, especially for low static magnetic field or samples of low gyromagnetic ratio.

Although FDNMR is a promising method for micro-NMR sensing, some issues need to be considered for the implementation. First, how is the structure realized using MEMS techniques? The whole system consists of two magnets, a cantilever, and a microcoil. It is more complicated than the system that is designed using the IDNMR approach, in which the fabrication of a microcoil and the electronics is much easier, but circuit design is more complicated. Second, what material is suitable for making the magnets? A material must be found that has low-density, high residual induction and is also appropriate for the fabrication process. Finally, how much uniformity of magnetic field across the sample can be achieved with the annular slot between two magnets? This is important in BOOMERANG since we can utilize the signal coming from the whole sample only when the magnetic field across the sample is uniform.

Acknowledgement

The authors would like to thank Irving Lowe, Jason Hsu, Irving Oppenheim, Paul J. Sides, and James H. Garrett for their suggestions on this work. This research is supported by the National Science Foundation.

Reference

1. J. A. Sidles, “Noninductive detection of single-proton magnetic resonance,” *Applied Physics Letter*, Vol. 58, no. 24, pp. 2854-2856, 1991.

2. N. Nestle, A. Schaff, and W. S. Veeman, “Mechanically detected NMR, an evaluation of applicability for chemical investigations,” *Progress in Nuclear Magnetic Resonance Spectroscopy*, vol. 38, no. 1, pp. 1-35, 2001.

3. R. L. Magin, A. G. Webb, and T. L. Peck, “Miniature magnetic resonance machines,” *IEEE Spectrum*, vol. 34, no. 10, pp. 51-61, 1997.

4. T. L. Peck, R. L. Magin, J. Kruse and M. Feng, "NMR microspectroscopy using 100 μm planar RF coils fabricated on gallium arsenide substrates," *IEEE Trans. Biomedical Eng.*, vol. 41, no. 7, pp. 706-709, 1994.

5. J. E. Stocker, T. L. Peck, A. G. Webb, and R. L. Magin, "Nanoliter volume, high-resolution NMR microspectroscopy using a 60 μm planar microcoil," *IEEE Trans. Biomedical Eng.*, vol. 44, no. 11, p.p. 1122-1127, 1997.

6. G. Boero, C. de Raad Isei, P. A. Besse, and R. S. Popovic, "An NMR magnetometer with planar microcoils and integrated electronics for signal detection and amplification," *Sensors and Actuators A*, vol. 67, pp. 18-23, 1998.

7. G. Boero, "Integrated NMR probe for magnetometry," Ph.D. thesis, Institute of Microsystem, Swiss Federal Institute of Technology (EPFL), Lausanne, Switzerland, June 2000.

8. D.I. Hoult and R.E. Richards, "The signal-to-noise ratio of the nuclear magnetic resonance," *Journal of Magnetic Resonance*, vol. 24, pp. 71-85, 1976.

9. A.G. Webb, "Radiofrequency microcoils in magnetic resonance," *Progress in Nuclear Magnetic Resonance*, vol. 31, pp. 1-42, 1997

10. T.L. Peck, R.L. Magin, and P.C. Lauterbur, "Design and analysis of microcoils for NMR microscopy," *Journal of Magnetic Resonance*, series B, vol. 108, pp. 114-124, 1995.

11. D. Rugar, C.S. Yannoni, and J.A. Sidles, "Mechanical detection of magnetic resonance," *Nature*, vol. 360, no. 10, pp. 563-566, 1992.

12. D. Rugar et al., "Force detection of nuclear magnetic resonance," *Science*, vol. 264, pp. 1560-1563, 1994.

13. K. Wago et al., "Low temperature magnetic resonance force detection," *Journal of Vacuum Science Technology B*, vol.14, pp.1197, 1996.

14. G.M. Leskowitz, L.A. Madsen, and D.P. Weitekamp, "Force-detected magnetic resonance without field gradients," *Solid State Nuclear Magnetic Resonance*, vol. 11, pp. 73-86, 1998.

15. C.S. Yannoni, O. Zuger, D. Rugar, and J.A. Sidles, "Force detection and imaging in magnetic resonance," *Encyclopedia of Nuclear Magnetic Resonance*, New York, Wiley, 1996.

16. A. Abragam, *The Principles of Nuclear Magnetism*, Oxford University Press, London, 1961.

17. J.D. Jackson, *Classical Electrodynamics*, 2nd ed., Wiley, New York, 1975.

18. W.C. Young and R.J. Roark, *Roark's Formulas for Stress and Strain*, 6th ed., McGraw-Hill, New York, 1989.

19. R.M. Bozorth, *Ferromagnetism*, IEEE Press, New York, pp. 873, 1993.

20. J.D. Kraus, *Electromagnetics*, 4th ed., McGraw-Hill, New York, 1991.